RSC Advances

ROYAL SOCIETY OF CHEMISTRY

www.rsc.org/advances

The successive photocurrent transient study to probe the sub-band gap electron and hole traps in ZnO nanorods

Dipanwita Sett, Sanjit Sarkar and Durga Basak*

Department of Solid State Physics, Indian Association for the Cultivation of Science, Jadavpur, Kolkata 700032, India

Persistent photoconductivity and spectral response corresponding to sub-band gap energies of ZnO as a result of different defects though certainly problematic characteristics, study on this however, is quite useful in the sense that it provides information about the defects levels. A developed understanding of the energetic distributions of sub-band gap electron and hole traps in ZnO nanorods is pre-requisite for device applications and needs to be acquired primarily. Through a study on simple successive photocurrent transients of as grown and annealed aqueous chemically grown ZnO nanorods, we have revealed the sub-band gap electron and hole traps responsible for visible photoresponse. The evolutions in the room temperature photoluminescence properties of ZnO NRs with annealing temperature have also been investigated critically to correlate the corresponding photocurrent results. As-grown samples show fewer amounts of excess O related electron trap states at $\leq E_c$-1.77 eV. More amount of O vacancy related hole traps as well as fewer amount of O interstitials related electron traps at $\leq E_c$-2.34 eV have been detected in as-grown as compared to the annealed samples. These findings also provide general guidelines for probing sub-band gap traps, and engineering the optoelectronic properties of similar oxide semiconducting nanoparticles.

*Corresponding author: email-sspdb@iacs.res.in

Introduction

Recent progress in the synthesis and characterization of nanosized ZnO particles have been driven by their potential application in fabricating nanoscale optoelectronic and electronic devices such as short wavelength light emitting and laser diodes, UV photodetectors, solar cells, transistors[1-8] due to its wide and direct band gap of 3.37 eV, large exciton binding energy of 60 meV, high electron mobility, low cost synthesis, ability to be etched by chemical techniques as compared other II-VI semiconductors. However, unlike many topics in the field of oxide semiconductors, it seems there is a tangled web of research and opinions when it comes to properties of ZnO and its defects. Therefore, an understanding of its sub-band gap electron and hole trap levels is important and essential in a number of areas of device design.[9-13] Two examples are the tailoring of photo response to particular spectral regions and the use of photocurrent spectroscopy as well as transient (photocurrent growth-decay with time) as a strong tool to probe the electronic energy-band structures of other similar useful wide band gap semiconductors such as TiO_2, SnO_2.[14-17] Despite the above demand, little work has been done on measuring and interpreting the electronic transitions in ZnO nanostructures particularly using photocurrent spectrum, photocurrent transients and derivative of photocurrent spectroscopic data. In this letter, we present data on optical transitions, observed by photocurrent spectroscopy and consecutive trap vacating by variable excitations (first with red, then with green and finally with UV lights) in aqueous chemically grown (ACG) ZnO nanorods (NRs). The concept of successive excitation with light of two different wavelengths for probing the sub-band gap defects for ZnO is not reported earlier and we believe our work presenting the application of this simple and sensitive technique to probe the traps and correlation with the emissions in ZnO nanostructures will provide a deep insight in the area. Further use of the derivative of the photocurrent spectroscopy data helps to locate the transitions and resolve the closely spaced features that are present in ZnO, a material with a very complicated defect band structures. In conjunction with the photocurrent measurements, first we have made a careful analysis of the emission evolutions in the photoluminescence (PL) spectra of the as-grown and annealed samples. The ZnO luminescence spectrum consists of a sharp UV and a broad visible emission bands. One or more emission peaks in the visible region is attributed to different types of defects, the origin of which are still more confusing when different literatures are compared.[18-24] Considering the fact that correlation of the radiative recombination features with the optical transitions is essential for

interpreting the optical data,[25-28] we have first probed the sub-band gap electron hole traps via successive photocurrent transients by exciting ZnO NRs with red, green and UV lights followed by an assignment through intricate correspondence between the PL and photoconductivity (PC) features in as-grown and annealed samples. A qualitative band model has been proposed based on the results.

Experimental section

The samples studied were grown on pre-cleaned glass substrates by the ACG method following a method described elsewhere.[29] In brief, at first, a seed layer of ZnO was deposited on the substrates and then the NRs were grown by dipping the substrates in a mixture of zinc acetate and hexamethylenetetramine at 80 ^{0}C for 1 hour. The substrates were then removed, cleaned and dried. The ZnO NRs were annealed at 200 ^{0}C, 300 ^{0}C and 500 ^{0}C in air ambient.

The structural and morphological confirmations were done by using X-ray diffractometer (Bruker, model D8) and field emission electron microscopy (JEOL, model JEM2010). A He-Cd laser (Kimmon Koha Co., Ltd.; model KR1801C) with a wavelength of 325 nm was used for the optical excitation of the sample. A high-resolution spectrometer (Horiba Jobin Yvon, Model: iHR 320) together with a photomultiplier tube was used to detect PL emissions from the samples. For the purpose of photocurrent measurements, two gold metal electrodes (40 nm thickness) were deposited in circular form with a diameter of 1 mm through a shadow mask at a separation of 3 mm on the top surface of the NRs using a thermal evaporator. The photocurrents were measured by illuminating the NRs with a monochromatic light from a 150 W Xenon (model 66902) lamp under 5 V bias conditions using a Keithley source meter (model 2400). The photocurrent spectrum was measured by illuminating the sample for 4 minutes with a light of varying wavelength from 800 nm to 300 nm and recording the corresponding current. Prior to measure the photocurrent, the samples were brought to equilibrium by keeping them in dark for long hours.

Results and discussion

Fig. 1 shows the XRD patterns of as-grown as well as annealed ZnO NRs. The patterns show the diffraction peaks corresponding to the typical hexagonal wurtzite structure of ZnO. Formation of highly oriented as-grown and annealed ZnO NRs along C axis on the glass

substrates has been observed. The XRD patterns further show that neither there is any change in the peak positions of the wurtzite structure after annealing nor any other peak suggesting that the ZnO NRs retain the similar phase and purity. Interestingly, as contrast to polycrystalline bulk, in this case, annealing causes reduction in the intensity of the XRD peaks. This is quite expected for ZnO as the defects segregate just below the crystallite surface of its one dimensional nanostructures having large surface-to-volume ratio, which often become the binding centers for the surface adsorbed species like O_2, –OH, H_2 etc.[30-31] However, these defects increase or decrease depending on the annealing ambient. In the as-grown NRs, due to the segregated defects on the surface, the bulk forming the inside of the NRs becomes devoid of defects and thus intense XRD peaks result. After annealing at lower temperatures, –OH desorbs, and a decrease in the XRD peak intensity has been observed. At higher temperature, H_2 desorbs from the surface making V_{Zn} type of defects mobile thus making the bulk of the crystallites inferior.[32-33] This causes less intense XRD peaks after annealing. There is also a possibility of competitive effect from various defects which is not understood at the moment.

Further, support of the fact that the undoped and doped ZnO NRs have been grown vertically on the substrate has been obtained from the inset in fig. 2(a). The FESEM images show that the NRs have a diameter in the range of 41-44 nm and length in the range of 300 nm -500 nm for all samples (Fig. 2). There is no much change in the morphology of the NRs occurs after the thermal treatment except that 300 ^{O}C and 500 ^{O}C annealed samples show little agglomeration as compared to as-grown and 200 ^{O}C annealed samples. Our NRs are not perfectly vertical but quasi vertical (the inset in Fig. 2(a)). Therefore, the tips touching each other in few places are likely to be joined together upon annealing.

PL and PC are two complementary processes. PL results from the radiative recombinations only while photoconductivity arises due to both radiative and nonradiative optical transitions. Fig. 3 shows the PC spectra of the as-grown and annealed ZnO NRs in the "ordinary" mode. These spectra have not been corrected for the spectral dependence of the source intensity, The spectra in general show a sharp peak below 400 nm due to the band gap absorption and generation of photocarriers and a broad hump in the wavelength 450-750 nm due to photocarriers released from different sub-band gap defect states contributing to the corresponding PCs. The spectrum for 200 ^{0}C annealing shows a lesser current both in the visible and UV regions. With an increase in the annealing temperature, current also increases in the

visible region especially around 430 nm to 650 nm, indicating formation of more defect states in the ZnO NRs. Ratios of I_{ph} at 370 nm to I_{ph} at 570 nm (Table-I) show that initially there is a tendency for a rise and then a fall in the ratio which indicates first a betterment and then a degradation in the quality which is at par with the PL results (discussed later). As such, features for and near band gap spectral region will not be discussed further as we are interested in sub-band gap levels.

All the PC curves in Fig. 3 show two maximum changes in the spectrum (i.e rise in the PC) one beyond 700 nm and one at around 570 nm. Therefore to identify the electron traps responsible for these changes, the PC transient experiments were performed by exciting the NRs first with 700 nm (red, 1.77 eV) light, then with 540 nm (green, 2.34 eV) light and finally with the 360 nm (UV) light, each for 15 min, in order to vacate the traps as per their energy band positions below the CB. The fig. 4(a) shows that the PC increases for all the samples as soon as 700 nm red light (1.77 eV) is shined. According to the PC spectra, it can be inferred that the carriers are released from the trap levels having energy $\leq E_c$ -1.77 eV. To estimate this effect, for simplicity, we have assumed that the predominant effect is occurring due to one type of traps. The values of photo-to-dark current ratio i.e PC gain for red light (I_{red}/I_{dc}) is $1.54x10^2$ for as-grown and are $1.47x10^3$, $1.8x10^3$ and $1.48x10^3$ respectively for the annealed NRs (Table-I). The values suggest that maximum release of the trapped electron occurs in the annealed samples making the ratio higher in the later as compared to the as-grown samples. Similarly, maximum carrier release under UV excitation after red and green excitation occurs in asgrown sample. Given the condition of annealing (atmosphere), excess O and/or O_i (oxygen interstitial) related two defects are most likely to be formed. Presumably excess O trap occurs at $\leq E_c$-1.77 eV which causes the optical transition since the other defect, O_i is well known to form a level 2.28 eV below the CB.[34-35] The agreement with proposition can be improved further by accounting the percentage values of the released carriers (proportional to the photocurrent) due to red light excitation (N_{red}) with the annealing temperature which shows a nonlinear increasing trend in the carriers as the annealing temperature increases (Table-I).

We find interesting changes occurring for the samples under steady green light excitation. For the as-grown sample, there is no increase at all under 2.34 eV excitation, rather a fall in the photocurrent has been observed (Fig. 4(b)) resulting in a negative change in the PC. It indicates existence of a sub-band gap hole as well as an electron trap at $\leq E_c$-2.34 eV. Trap-assisted recombination occurs when an electron falls and occupy a "trap", and in a second step, moves

into an empty valence band state, thereby completing the recombination process referred as Shockley-Read-Hall (SRH) recombination.[36] Our transient curve in Fig. 4(a) indicates that these hole traps are much more in number in the as-grown sample, so that the recombinations in these compensates the reduction by the excitation of holes from traps to the VB. On the contrary for the annealed samples, Fig. 4(a) shows an initial increase and then a decrease in the photocurrent forming a 'kink' feature which increases as annealing is done at higher and higher temperatures (Fig. 4(b)). It indicates that in the annealed samples, number of hole traps are reduced so that under excitation of 2.34 eV light, initially electrons are released from the levels lying within (E_c - 1.77 eV) and (E_c-2.34eV) but soon hole release dominates resulting in an exponential decay in the current. Since O_i cannot be an electron trap as it is already negatively charged, the electron trap in this case most probably is V_OZn_i i.e (E_c-2.16 eV).[32] Next, what could be the origin of the hole traps? As the number of hole traps are decreased in the annealed samples, in all possibility, the hole traps may be V_O defects (neutral or singly ionized). The explanation is as follows: O_i forms in ZnO as per equation $O_O = V_O + O_i$ and V_O-O_i pair forms.[37] In an annealing process because of the oxygen ambient and O_i formation, the absorption of O atoms counteracts the formation of V_O-O_i pairs and pushes the O_i atoms back to the sites of V_O reducing the number of V_O which is at par with the decrease in hole traps. According to energy calculation and experimental results, the amount of V_O in n-type ZnO is quite less in equilibrium condition as its formation energy is very high.[38-39]

The PL spectra of the as-grown and annealed ZnO NRs (Fig. 5) mainly consist of a UV emission peak at ~380 nm and one or more visible band/peaks. The intensity of the UV peak associated with free-exciton recombination across the band gap is mostly dependent on the visible emission intensity.[40] The UV/VIS ratio is 1.14 for as-grown and the values are 2.21, 3.21 and 0.96 respectively for the annealed (200 ^{0}C, 300 ^{0}C and 500 ^{0}C) NRs which means that the UV/VIS ratio increases for 200 ^{0}C, 300 ^{0}C but the ratio decreases for 500 ^{0}C annealed sample. The FWHM of the UV peak (Table-I) slightly decreases for 200 ^{0}C, 300 ^{0}C while the value increases for 500 ^{0}C annealing. Both the changes in the intensity as well as in the FWHM values can be understood easily. The enhancement of the UV peak intensity after annealing at and above 200 ^{0}C is probably due to the desorption of hydroxyl groups at ~150 ^{0}C.[41] Therefore, by heating at 200 ^{0}C and 300 ^{0}C temperature, all the surface states related to OH groups or $Zn(OH)_2$ goes off which results in more intense UV emission as compared to the visible emission. The as-grown and 200 ^{0}C annealed sample show a broad visible band with a peak at ~566 nm (yellow

emission) which is assigned due to the presence of O_i.[30] The peaks shifts towards higher wavelength i.e orange component of the emission can be observed after annealing at 300 ^{0}C temperature. Red shift of the visible peak and its enhanced intensity occurs in 300 ^{0}C annealed sample due to radiative recombination via V_O defects which is similar with the findings observed by Djurisic et al.[24] The results are in good agreement with the PC results during green excitation which also indicates presence of V_O–related defects. H_2 desorbs at ~420 ^{0}C.[42] H_2 mainly passivate zinc vacancies (V_{zn}) type of surface defects and helps to achieve an intense UV emission. So, annealing at 500 ^{0}C releases adsorbed H_2 for which V_{Zn} defects become mobile within the crystal lattice worsening the FWHM value as well as the UV intensity.[43] Annealing at higher temperature, the green emission dominates which is predominant contribution of V_{Zn}.[44-47] In other words, as per PC results, V_O cannot be the origin of green emission. Therefore, an orange component at 610 nm appears probably due to V_O^+.[48-49]

Remarkably good agreement between the PL and the derivative of PC (DPC) spectrum clearly identify the electron and hole traps. The dI/dλ is a useful and sensitive technique to pin optical transition levels. Fig. 6(a) shows that there are three peaks in the PL spectrum at 2.03 eV (orange), 2.25 eV (yellow) and 2.42 eV (green). In the dI/dλ curve of 500 ^{0}C annealed sample, there are 'dip' features at 1.93 eV, 2.06 eV, 2.29 eV, 2.58 eV. The dips indicate either electron trap and/or hole release and/or recombinations. Matching and correlating both PL and DPC, the presence of a hole trap (V_O-related) at ~2.06 eV, recombination centres at ~2.25-2.29 eV (O_i) and 2.43-2.58 eV (V_{Zn}) are confirmed. The latter two therefore respectively can be correlated to the yellow and green emissions. Based on the above results, an energy band diagram of these ZnO NRs has been proposed in Fig. 6(b).

Conclusions

In summary, the sub-band gap photocurrent spectra, successive photocurrent transient spectroscopy and derivative of the photocurrent transient spectrum of asgrown and annealed ACG ZnO NRs have been analyzed. The as-grown NR samples show fewer amount of excess O related electron trap states at (E_c-1.77 eV) and more number of O vacancy related hole traps as well as fewer O interstitials related electron traps at (E_c-2.34 eV) as compared to the annealed samples. An intricate correlation between the PL and PC features in asgrown and annealed samples have been done and accordingly a band model has been proposed showing qualitatively the electron and hole traps.

Acknowledgements

The authors thank CSIR for funding the work vide project no: 03(1260)/12/EMR-II. The authors, D. Sett and S. Sarkar thank CSIR, India for providing the fellowships.

References

1 M. Afsal, C. Y. Wang, L. W. Chu, H. Ouyang and L. J. Chen, J. Mater. Chem., 2012, **22**, 8420-8425.

2 M. H. Huang, S. Mao, H. Feick, H. Q. Yan, Y. Y. Wu, H. Kind, E. Weber, R. Russo and P. D. Yang, Science, 2001, **292**, 1897-1899.

3 J. J. Qi, X. F. Hu, Z. Z. Wang, X. Li, W. Liu and Y. Zhang, Nanoscale, 2014, **6**, 6025-6029.

4 S. Y. Ju, A. Facchetti, Y. Xuan, J. Liu, F. Ishikawa, P. D. Ye, C. W. Zhou, T. J. Marks and D. B. Janes, Nat. Nanotechnol., 2007, **2**, 378-384.

5 Y. Qin, X. D. Wang and Z. L. Wang, Nature, 2008, **451**, 809-U805.

6 S. F. Varol, D. Sahin, M. Kompitsas and G. Cankaya, RSC Adv., 2014, **4**, 13593-13600.

7 H. Shen, C. X. Shan, Q. Qiao, J. S. Liu, B. H. Li and D. Z. Shen, J. Mater. Chem. C, 2013, **1**, 234-237.

8 Y. Z. Zheng, J. X. Zhao, H. Zhang, J. F. Chen, W. L. Zhou and X. Tao, Chem. Commun., 2011, **47**, 11519-11521.

9 X. L. Wu, S. J. Xiong, Z. Liu, J. Chen, J. C. Shen, T. H. Li, P. H. Wu and P. K. Chu, Nat. Nanotechnol., 2011, **6**, 102-105.

10 C. Soci, A. Zhang, B. Xiang, S. A. Dayeh, D. P. R. Aplin, J. Park, X. Y. Bao, Y. H. Lo and D. Wang, Nano Lett., 2007, **7**, 1003-1009.

11 F. W. Guo, B. Yang, Y. B. Yuan, Z. G. Xiao, Q. F. Dong, Y. Bi and J. S. Huang, Nat. Nanotechnol., 2012, **7**, 798-802.

12 K. Chung, C. H. Lee and G. C. Yi, Science, 2010, **330**, 655-657.

13 C. Chen, H. P. He, Y. F. Lu, K. W. Wu and Z. Z. Ye, ACS Appl. Mater. Interfaces, 2013, **5**, 6354-6359.

14 D. Flak, A. Braun, B. S. Mun, J. B. Park, M. Parlinska-Wojtan, T. Graule and M. Rekas, Phys. Chem. Chem. Phys., 2013, **15**, 1417-1430.

15 C. Richter and C. A. Schmuttenmaer, Nat. Nanotechnol., 2010, **5**, 769-772.

16 Y. F. Li, R. Deng, Y. F. Tian, B. Yao and T. Wu, Appl. Phys. Lett., 2012, **100**, 172402.

17 G. Rahman, N. U. Din, V. M. Garcia-Suarez and E. Kan, Phys. Rev. B, 2013, **87**, 205205.

18 H. X. Chen, J. J. Ding, W. G. Guo, G. X. Chen and S. Y. Ma, RSC Adv., 2013, **3**, 12327-12333.

19 S. Dhara and P. K. Giri, Nanoscale Res. Lett., 2011, **6**, 504.

20 M. J. Li, G. C. Xing, G. Z. Xing, B. Wu, T. Wu, X. H. Zhang and T. C. Sum, Phys. Rev. B, 2013, **87**, 115309.

21 A. Layek, B. Manna and A. Chowdhury, Chem. Phys. Lett., 2012, **539**, 133-138.

22 J. Kossmann and C. Hattig, Phys. Chem. Chem. Phys., 2012, **14**, 16392-16399.

23 P. S. Venkatesh, V. Purushothaman, S. E. Muthu, S. Arumugam, V. Ramakrishnan, K. Jeganathan and K. Ramamurthi, Crystengcomm, 2012, **14**, 4713-4718.

24 A. B. Djurisic, Y. H. Leung, K. H. Tam, Y. F. Hsu, L. Ding, W. K. Ge, Y. C. Zhong, K. S. Wong, W. K. Chan, H. L. Tam, K. W. Cheah, W. M. Kwok and D. L. Phillips, Nanotechnology, 2007, **18**.

25 S. Dhara and P. K. Giri, J. Appl. Phys., 2011, **110**, 124317.

26 S. K. Mishra, R. K. Srivastava, S. G. Prakash, R. S. Yadav and A. C. Panday, Opto-Electron. Rev., 2010, **18**, 467-473.

27 S. Dhara and P. K. Giri, J. Appl. Phys., 2012, **111**, 044320.

28 S. Panigrahi and D. Basak, Nanoscale, 2011, **3**, 2336-2341.

29 A. Bera, T. Ghosh and D. Basak, ACS Appl. Mater. Interfaces, 2010, **2**, 2898-2903.

30 P. P. Das, S. A. Agarkar, S. Mukhopadhyay, U. Manju, S. B. Ogale and P. S. Devi, Inorg. Chem., 2014, **53**, 3961-3972.

31 X. Y. Xu, C. X. Xu, Y. Lin, J. T. Li and J. G. Hu, J. Phys. Chem. C, 2013, **117**, 24549-24553.

32 K. H. Tam, C. K. Cheung, Y. H. Leung, A. B. Djurisic, C. C. Ling, C. D. Beling, S. Fung, W. M. Kwok, W. K. Chan, D. L. Phillips, L. Ding and W. K. Ge, J. Phys. Chem. B, 2006, **110**, 20865-20871.

33 J. J. Zhang, E. J. Guo, L. P. Wang, H. Y. Yue, G. J. Cao and L. Song, Trans. Nonferrous Met. Soc. China, 2014, **24**, 736-742.

34 S. Kuriakose, B. Satpati and S. Mohapatra, Phys. Chem. Chem. Phys., 2014, **16**, 12741-12749.

35 A. B. Djurisic and Y. H. Leung, Small, 2006, **2**, 944-961.

36 A. Schenk, Solid-State Electron., 1992, **35**, 1585-1596.

37 H. B. Fan, S. Y. Yang, P. F. Zhang, H. Y. Wei, X. L. Liu, C. M. Jiao, Q. S. Zhu, Y. H. Chen and Z. G. Wang, Chin. Phys. Lett., 2007, **24**, 2108-2111.

38 A. Janotti and C. G. Van de Walle, Phys. Rev. B, 2007, **76**, 165202.

39 F. Tuomisto, K. Saarinen, D. C. Look and G. C. Farlow, Phys. Rev. B, 2005, **72**, 085206.

40 A. van Dijken, E. A. Meulenkamp, D. Vanmaekelbergh and A. Meijerink, J. Lumines., 2000, **87-9**, 454-456.

41 Y. F. Yao, C. H. Shen, W. F. Chen, P. Y. Shih, W. H. Chou, C. Y. Su, H. S. Chen, C. H. Liao, W. M. Chang, Y. W. Kiang and C. C. Yang, J. Nanomater., 2014, 756401.

42 R. G. Xie, T. Sekiguchi, T. Ishigaki, N. Ohashi, D. S. Li, D. R. Yang, B. D. Liu and Y. S. Bando, Appl. Phys. Lett., 2006, **88**, 134103.

43 A. Bera and D. Basak, Appl. Phys. Lett., 2009, **94**, 163119.

44 A. Janotti and C. G. Van de Walle, Rep. Prog. Phys., 2009, **72**.

45 F. Fabbri, M. Villani, A. Catellani, A. Calzolari, G. Cicero, D. Calestani, G. Calestani, A. Zappettini, B. Dierre, T. Sekiguchi and G. Salviati, Sci Rep, 2014, **4**, 5158.

46 Y. H. Leung, X. Y. Chen, A. M. C. Ng, M. Y. Guo, F. Z. Liu, A. B. Djurisic, W. K. Chan, X. Q. Shi and M. A. Van Hove, Appl. Surf. Sci., 2013, **271**, 202-209.

47 J. P. Lv, C. D. Li and J. J. BelBruno, Crystengcomm, 2013, **15**, 5620-5625.

48 A. B. Djurisic, Y. H. Leung, K. H. Tam, L. Ding, W. K. Ge, H. Y. Chen and S. Gwo, Appl. Phys. Lett., 2006, **88**, 103107.

49 Q. Zhu, C. S. Xie, H. Y. Li, C. Q. Yang, S. P. Zhang and D. W. Zeng, J. Mater. Chem. C, 2014, **2**, 4566-4580.

TABLE I. The FWHM value of UV PL peak, UV/VIS ratio of UV and visible PL peak, ratio of I_{ph} at 370 nm and I_{ph} at 570 nm in PC spectra, photocurrent gain (I_{red}/I_{dc} and I_{UV}/I_{dc}), percentage released carriers due to red excitation (N_{red}) of as-grown and annealed ZnO NRs.

Annealing temperature	FWHM of UV PL peak	UV/VIS	$I_{370\ nm}/I_{570\ nm}$	$G_r=I_{red}/I_{dc}$	$G_{UV}=I_{UV}/I_{dc}$	$N_{red}=(G_r/G_{UV})\times 100$
As-grown	19.61	1.14	4.05	1.54×10^2	2090	7.36
200 ^{0}C	18.31	2.21	7.16	1.47×10^3	16515	8.90
300 ^{0}C	16.54	3.21	2.63	1.8×10^3	14949	12.04
500 ^{0}C	22.73	0.96	2.86	1.48×10^3	5700	25.96

Figure captions:

Fig. 1. XRD patterns of as-grown (a) and 200 ^{0}C (b), 300 ^{0}C (c), 500 ^{0}C (d) annealed ZnO NRs.

Fig. 2. FESEM images of as-grown (a) and 200 ^{0}C (b), 300 ^{0}C (c), 500 ^{0}C (d) annealed ZnO NRs. The inset in Fig. 2(a) shows a tilted view of the quasi vertical NRs.

Fig. 3. PC spectra of as-grown (a) and 200 ^{0}C (b), 300 ^{0}C (c), 500 ^{0}C (d) annealed ZnO NRs. The inset shows the schematic diagram for the photocurrent measurement set-up.

Fig. 4. (Top) Transient PC response of as-grown and 200 ^{0}C (b), 300 ^{0}C (c), 500 ^{0}C (d) annealed ZnO NRs, (Bottom) Magnified view of the encircled portion of the curves in the top graph.

Fig. 5. PL spectra of as-grown (a) and 200 ^{0}C (b), 300 ^{0}C (c), 500 ^{0}C (d) annealed ZnO NRs.

Fig. 6. (a) PL spectra and the derivative of PC (DPC) of ZnO NRs annealed at 500 ^{0}C, (b) Qualitative schematic of the energy band diagram of ZnO NRs.

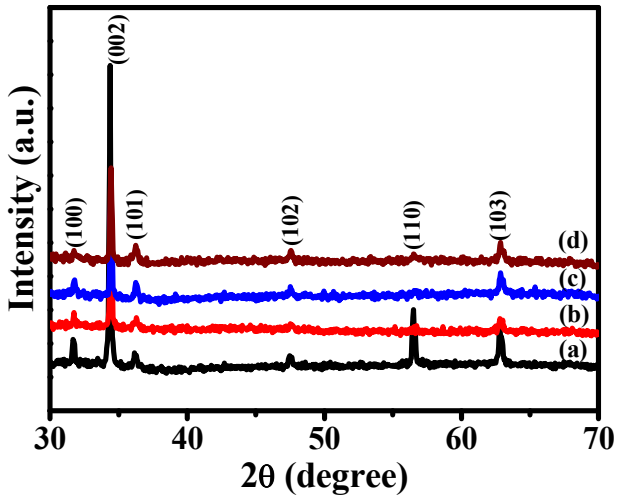

Fig. 1

Sett et al.

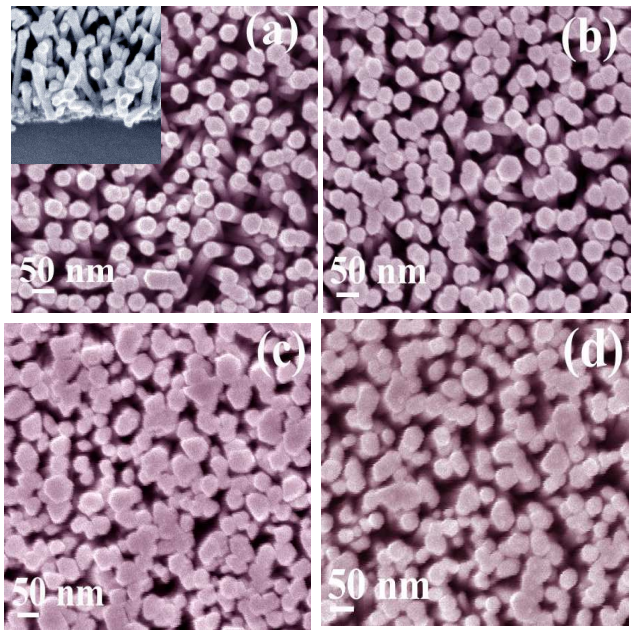

Fig. 2

Sett et al.

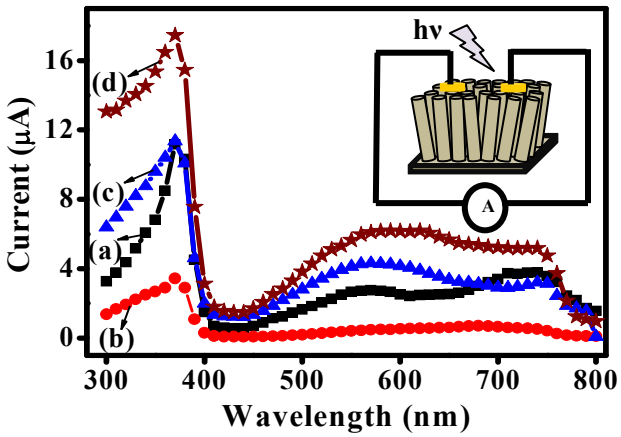

Fig. 3

Sett et al.

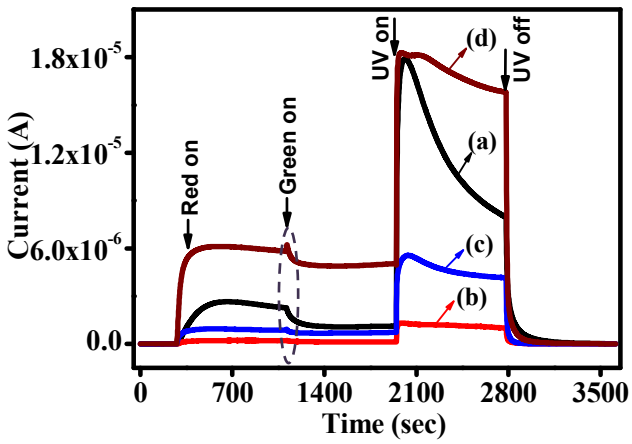

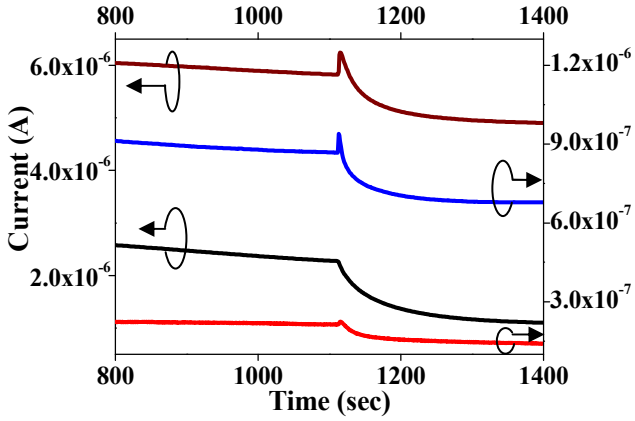

Fig. 4

Sett et al.

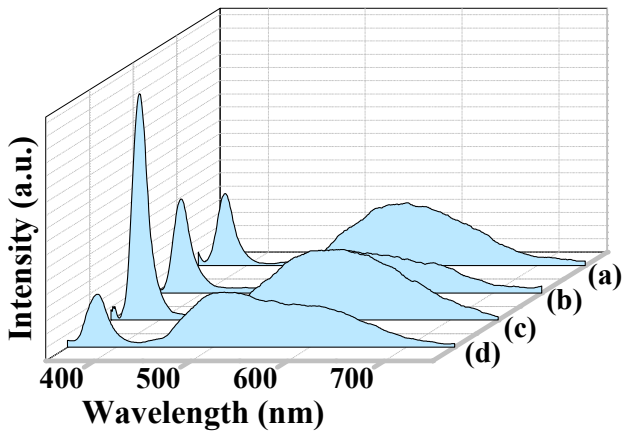

Fig. 5

Sett et al.

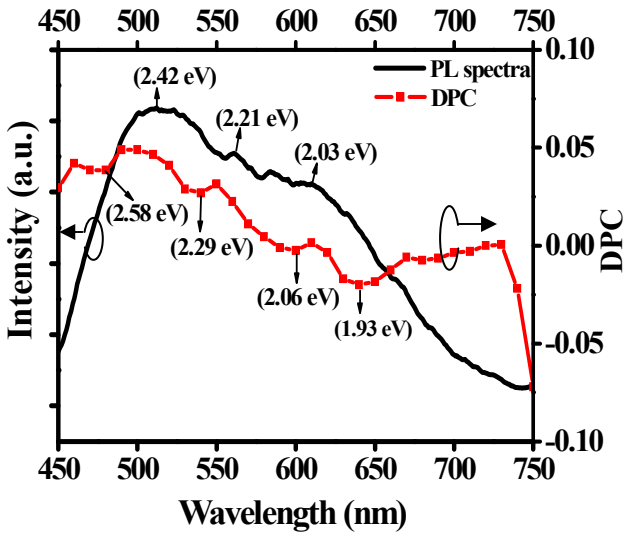

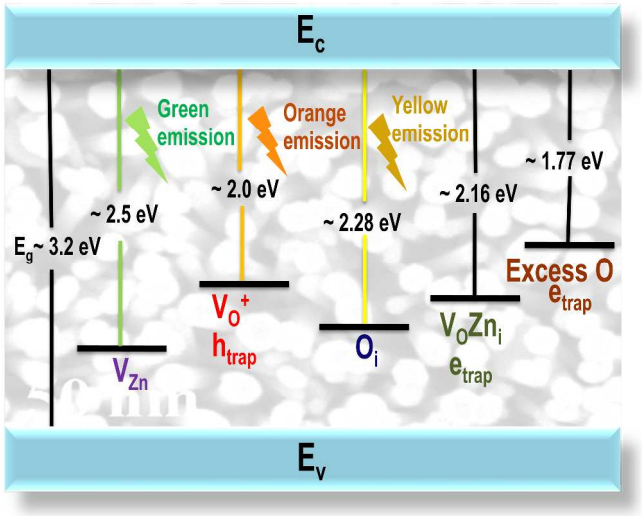

Fig. 6

Sett et al.